Leaf senescence is accompanied by an early disruption of the microtubule network in Arabidopsis

Olivier Keech, Edouard Pesquet, Laurent Gutierrez, Abdul Ahad, Catherine Bellini, Steven M Smith, Per Gardestrom

Leaf Senescence Is Accompanied by an Early Disruption of the Microtubule Network in Arabidopsis[1][C][W]

Olivier Keech*, Edouard Pesquet, Laurent Gutierrez, Abdul Ahad, Catherine Bellini, Steven M. Smith, and Per Gardeström

Australian Research Council Centre of Excellence in Plant Energy Biology and Centre of Excellence for Plant Metabolomics, University of Western Australia, Crawley, Western Australia 6009, Australia (O.K., S.M.S.); Umea Plant Science Centre, Department of Plant Physiology, Umea University, SE–901 87 Umea, Sweden (E.P., P.G.); Centre de Ressources Régionales en Biologie Moléculaire, Université de Picardie Jules Verne, 80039 Amiens, France (L.G.); Umea Plant Science Centre, Department of Forest Genetics and Plant Physiology, Swedish University of Agricultural Sciences, SE–901 83 Umea, Sweden (L.G., C.B.); and Department of Botany, University of British Columbia, Vancouver, British Columbia, Canada V6T 1Z4 (A.A.)

The dynamic assembly and disassembly of microtubules (MTs) is essential for cell function. Although leaf senescence is a well-documented process, the role of the MT cytoskeleton during senescence in plants remains unknown. Here, we show that both natural leaf senescence and senescence of individually darkened Arabidopsis (*Arabidopsis thaliana*) leaves are accompanied by early degradation of the MT network in epidermis and mesophyll cells, whereas guard cells, which do not senesce, retain their MT network. Similarly, entirely darkened plants, which do not senesce, retain their MT network. While genes encoding the tubulin subunits and the bundling/stabilizing MT-associated proteins (MAPs) MAP65 and MAP70-1 were repressed in both natural senescence and dark-induced senescence, we found strong induction of the gene encoding the MT-destabilizing protein MAP18. However, induction of MAP18 gene expression was also observed in leaves from entirely darkened plants, showing that its expression is not sufficient to induce MT disassembly and is more likely to be part of a Ca^{2+}-dependent signaling mechanism. Similarly, genes encoding the MT-severing protein katanin p60 and two of the four putative regulatory katanin p80s were repressed in the dark, but their expression did not correlate with degradation of the MT network during leaf senescence. Taken together, these results highlight the earliness of the degradation of the cortical MT array during leaf senescence and lead us to propose a model in which suppression of tubulin and MAP genes together with induction of MAP18 play key roles in MT disassembly during senescence.

Leaf senescence can be the result of natural aging but can also be initiated in response to various stresses such as ozone, shading, or pathogen infection (Woolhouse, 1967; Smart, 1994). In response to these developmental or environmental cues, the leaf will undergo three distinct phases sequentially: (1) an initiation period, where metabolic changes lead to a decrease in photosynthetic activity and a transition from source to sink; (2) a degenerative phase, mainly characterized by the disassembly of cellular components and their degradation; and (3) a terminal phase, where cell integrity is lost prior to cell death and death of the whole organ (Nooden et al., 1997; Yoshida, 2003). As leaf senescence is also induced by abiotic and biotic stresses, understanding its mechanisms is not only important for answering fundamental scientific questions but also as part of a challenge to increase crop yields.

In a recent study with Arabidopsis (*Arabidopsis thaliana*; Keech et al., 2007), we showed that regulation of metabolism differed significantly between an individually darkened leaf (idl) attached to a whole plant and an equivalent leaf from an entirely darkened plant. After 6 d of darkness, photosynthetic capacity was maintained in leaves from a whole darkened plant, whereas the capacity for mitochondrial respiration decreased. In contrast, idls showed an accelerated senescence with a rapid decline in photosynthetic capacity, while mitochondrial capacity remained high. Additionally, we observed drastic ultrastructural alterations, including aggregation of both chloroplasts and mitochondria during the accelerated senescence occurring in mesophyll cells of idls. We consequently hypothesized that the cytoskeleton, and in particular the cortical microtubules (MTs), could undergo modifications contributing to the pronounced rearrange-

[1] This work was supported by the Australian Research Council (award nos. FF0457721 and CE0561495), by the Centres of Excellence program of the Government of Western Australia, and by the Swedish Foundation for International Cooperation in Research and Higher Education.

* Corresponding author; e-mail okeech@cyllene.uwa.edu.au.

The author responsible for distribution of materials integral to the findings presented in this article in accordance with the policy described in the Instructions for Authors (www.plantphysiol.org) is: Olivier Keech (okeech@cyllene.uwa.edu.au).

[C] Some figures in this article are displayed in color online but in black and white in the print edition.

[W] The online version of this article contains Web-only data.

www.plantphysiol.org/cgi/doi/10.1104/pp.110.163402

ments of the cellular content in the mesophyll cells during leaf senescence.

In plant cells, there are two main cytoskeleton components: (1) MTs, which are heterodimeric polymers of the globular proteins α- and β-tubulin; and (2) microfilaments, which are composed of actin monomers (Lloyd and Hussey, 2001; Boutté et al., 2007). MTs are assembled in a head-to-tail fashion to form protofilaments, and they are constantly undergoing polymerization and depolymerization at both the plus and minus ends (Hashimoto, 2003). They are mainly involved in cell elongation and cell division (Dixit and Cyr, 2004; Boutté et al., 2007), in the development of the plant cell wall, notably by facilitating or guiding cellulose deposition (Wasteneys, 2004; Lloyd, 2006; Wightman and Turner, 2008; Pesquet et al., 2010), and in organelle positioning (Van Gestel et al., 2002; Wada and Suetsugu, 2004; Romagnoli et al., 2007). Nevertheless, their function is intimately linked to their organizational state, which directly depends on the developmental and/or environmental conditions that the cells are facing (Dixit and Cyr, 2004). Modifications of these conditions trigger signals that, in turn, can be transduced through several types of proteins, generally referred to as microtubule-associated proteins (MAPs). MAPs, by their stabilizing, bundling, or severing activities, can then regulate the MT dynamics and can actively participate in the reorganization of the MT array (Lloyd and Hussey, 2001; Hashimoto and Kato, 2006; Hamada, 2007).

Although the dynamic assembly and disassembly of MTs is essential for cell stability and survival, the state of the MT cytoskeleton during senescence in plants remains largely unknown. Considering this in light of our previous data suggesting a remodeling of the cytoskeleton in leaves experiencing dark-induced senescence, we investigated changes in the cortical MT network and potential regulatory mechanisms during both natural and dark-induced leaf senescence in the model plant Arabidopsis.

RESULTS

Two Systems to Study Leaf Senescence

We compared attached leaves subjected to dark-induced senescence with Arabidopsis leaves naturally aging in order to assess whether the cytological modifications observed in our previous study (Keech et al., 2007) were dark induced or senescence specific. idls, previously described in detail by Weaver and Amasino (2001) and by Keech et al. (2007), offer a more synchronous and a better controlled process of senescence than age-induced senescence. Using this method in this work, we followed the progression of leaf senescence for 6 to 8 d, after which the leaves were yellow (Fig. 1A). Time zero idl (T0idl) represented leaves from 8-week-old plants with a chlorophyll content of 1.27 $\pm$ 0.04 mg mL^{-1} g^{-1} fresh weight. In parallel, from 11- to 13-week-old plants, we selected leaves at different stages of natural senescence (T0ns, T50ns, and T85ns). T0ns represented leaves with a chlorophyll content of 1.85 $\pm$ 0.02 mg mL^{-1} g^{-1} fresh weight, which was 30% more than in the T0idl. T50ns and T85ns were leaves undergoing natural senescence with approximately 50% and more than 85% reduction of their chlorophyll content, respectively. These three stages were consequently representative of the beginning, the middle, and the end of the process of natural senescence in Arabidopsis leaves (Fig. 1A). In addition, as we noticed that leaves undergoing natural senescence gen-

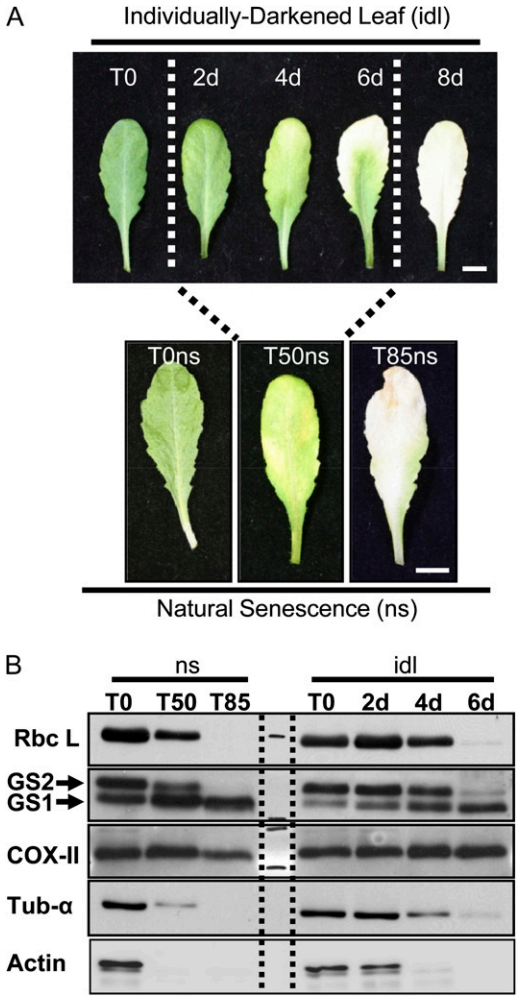

Figure 1. A, Representative time course of a mature rosette leaf of Arabidopsis plant undergoing either dark-induced senescence or natural senescence. For dark-induced senescence, leaves were individually darkened (idl) for 2 to 8 d. For natural senescence (ns), T50ns and T85ns represent 50% and at least 85% degradation of their chlorophyll content, respectively, in comparison with T0ns. Bars = 1 cm. B, Immunoblot analysis of total extracts from natural senescence (ns) and from idls (idl). Rubisco large subunit (Rbc L), Gln synthetase cytosolic (GS1) and chloroplastic (GS2) isoforms, cytochrome *c* oxidase subunit II (COX), α-tubulin (Tub-α), and F-actin (Actin) were tested. In each lane, 10 μg of protein was loaded.

erally exhibit a heterogeneous pattern of chlorosis (Supplemental Fig. S1), we proposed that T50ns could thus represent a combination of the three more distinct and more synchronous stages T2idl, T4idl, and T6idl, as suggested in Figure 1A.

To compare the similarities of the developmental stages between our two systems at the protein level, we ran immunoblot analyses with several relevant biological markers. In line with the progressive degradation of the chloroplasts during leaf senescence, the large subunit of Rubisco and the chloroplastic isoform of Gln synthetase (GS2) were progressively degraded during the two time courses of natural and dark-induced senescence (Fig. 1B). As expected, the relative content of the cytosolic isoform of Gln synthetase (GS1) increased during both natural and dark-induced senescence as part of the nitrogen remobilization and nutrient recycling pathway, in accordance with previous reports (Kawakami and Watanabe, 1988; Masclaux et al., 2000). It is worthwhile to note that the ratio GS1/GS2 was higher in T0ns leaves than in the T0idl leaves (Fig. 1B), reflecting an older stage of development of T0ns when compared with T0idl (see also quantitative real-time [qRT]-PCR analysis in Fig. 5C below). Mitochondrial degradation was tested with antibodies raised against cytochrome *c* oxidase subunit 2 (COX-II), the subunit of complex IV in the electron transport chain. We previously reported that the number of mitochondria per volume of leaf decreased during dark-induced senescence while their size increased (Keech et al., 2007). Here, we show that the amount of COX-II remained fairly stable during the 6 d of dark-induced and natural senescence, demonstrating that the ratio of mitochondrial proteins to total proteins remained almost unchanged during leaf senescence. This confirms that the degradation of mitochondria is slower than the degradation of chloroplasts and strengthens the prominent role of mitochondria during late events of leaf senescence, most likely to supply energy and the carbon skeleton to the cell for efficient nutrient remobilization. Finally, two cytoskeleton markers, α-tubulin for the MTs and actin for the actin filaments, decreased unexpectedly early during both dark-induced and natural leaf senescence.

In Vivo Visualization of the MT Cytoskeleton during Leaf Senescence

To investigate the consequences of such an early decrease in abundance of α-tubulin during both dark-induced (Fig. 2) and natural (Fig. 3) leaf senescence, the organization of the MT cytoskeleton was visualized in vivo by confocal laser microscopy using Arabidopsis plants constitutively expressing GFP-β-TUBULIN6 (*TUB6*; Nakamura et al., 2004). The GFP fusion to the N terminus of the Arabidopsis *TUB6* under the control of the cauliflower mosaic virus 35S promoter was demonstrated to be a reliable reporter to fluorescently label MTs in aerial tissues (Abe and Hashimoto, 2005). In addition, the authors reported

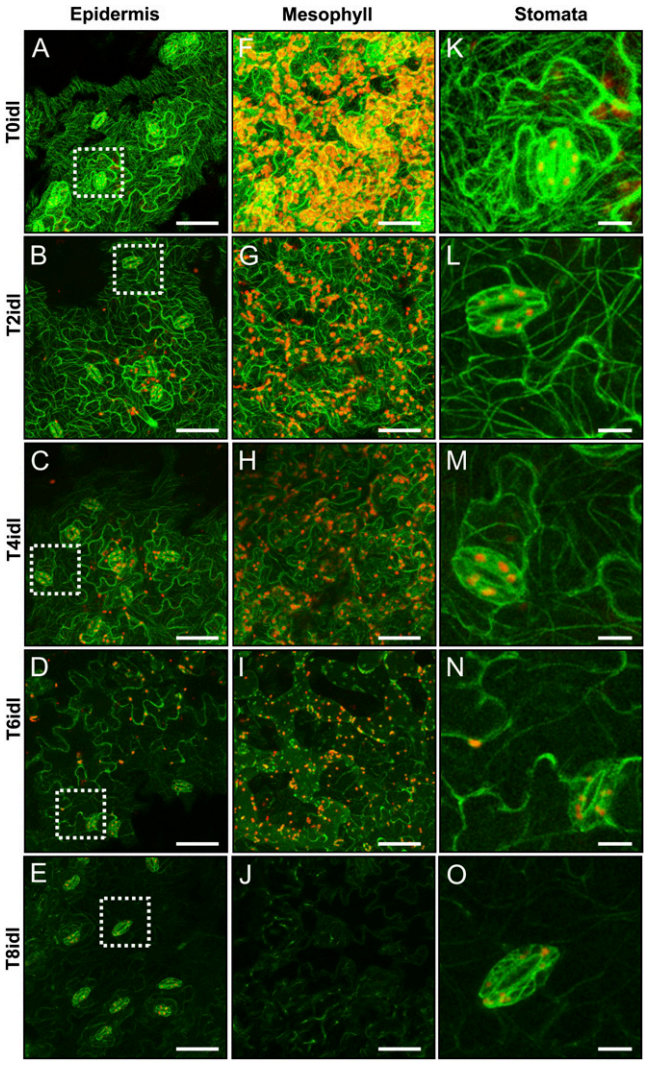

Figure 2. In folio imaging of the progressive disruption of MTs in epidermis (A–E), spongy mesophyll (F–J), and guard cells of stomata (K–O) during dark-induced senescence. Bars = 50 μm (A–J) and 10 μm (K–O).

the incorporation of labeled β-tubulin subunits to be 20% to 30% of the endogenous tubulin level. Thus, it is likely that the in vivo visualization of the polymerized MTs was unbiased, despite the construct being driven by a strong promoter. MTs were observed in three different cell types from the abaxial side of leaf sections. Already 2 d after the start of dark-induced senescence, a reduction of the MT network was observed in both the epidermis and the adjacent spongy mesophyll cells (Fig. 2, B and G), and this reduction was accentuated at 4 and 6 d in the two cell types. However, no apparent modification of the MT cytoskeleton was observed in guard cells of stomata (Fig. 2, K–O). We also noticed a progressive reduction in size and in number of chloroplasts in mesophyll cells (Fig. 2, F–I), which led to their complete degradation after 8 d (Fig. 2J). In line with our previous observations

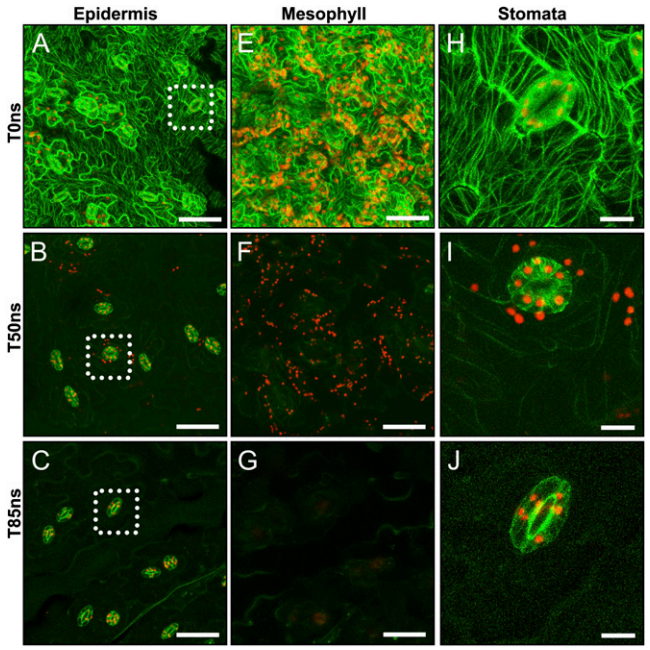

Figure 3. In folio imaging of the progressive disruption of MTs in epidermis (A–C), spongy mesophyll (E–G), and guard cells of stomata (H–J) during natural senescence. The late longevity of stomatal guard cells is evidenced by the conserved MT lattice (H–J). Bars = 50 μm.

(Keech et al., 2007), chloroplasts tended to aggregate after 6 d. Finally, after 8 d, the MT network was completely disrupted, with the exception of the stomatal guard cells, which retained both their MTs and their chloroplasts (Fig. 2, E, J, and O).

The situation was very similar in leaves undergoing natural senescence. The MT cytoskeleton from the epidermis and the mesophyll cells of T0ns leaves exhibited the same pattern as T0idl. Later, we observed a drastic reduction of the density of the MT cytoskeleton in epidermis and mesophyll cells after 50% degradation of the chlorophyll (T50ns; Fig. 3, B and F). After 85% degradation of the chlorophyll (T85ns), the depolymerization of the MTs was apparently complete in these two cell types (Fig. 3, C and G). We also noticed chloroplasts of a smaller size in mesophyll cells at T50ns (Fig. 3F) and their complete degradation at T85ns (Fig. 3G). Finally, as in dark-induced senescence, guard cells of stomata retained their MT network and their chloroplast until the very end of the leaf's life (Fig. 3, H–J).

Expression of Tubulin-Related Genes

In order to explain the progressive, tissue-dependent, disruption of the MTs during both dark-induced and natural senescence, we investigated the regulation of several molecular players that could be involved in the bundling/stabilization and the destabilization of the MT network. In Arabidopsis, there are six genes coding for α-tubulin subunits (Kopczak et al., 1992), nine for β-tubulin (Snustad et al., 1992), and two for γ-tubulin (Liu et al., 1994). From publicly available microarrays (van der Graaff et al., 2006) performed with leaves undergoing natural and dark-induced senescence in similar conditions to ours, we extracted relative expression profiles for all genes encoding tubulin subunits (Supplemental Table S3) and expressed the data as the $\log_2$ of the ratio between T25 T50, or T75 and the expression value of the gene at T0 (T0 being a 6-week-old leaf and T25, T50, and T75 being leaves with a loss of 25%, 50%, and 75% of their chlorophyll content, respectively). As shown in Figure 4, the expression pattern for the genes encoding α-, β-, and γ-subunits was fairly similar between natural (Fig. 4A) and dark-induced (Fig. 4B) senescence and showed a progressive repression for most of the genes. However, only a few of the genes showed a significant down-regulation. We subsequently used qRT-PCR to confirm that expression of *TUB6* matches that of van der Graaff et al. (2006) in our systems (Fig. 5).

While these results (van der Graaff et al., 2006) show reduced expression of the genes encoding tubulin subunits, we also hypothesized that other regulators could be involved in the disruption of the cortical MT

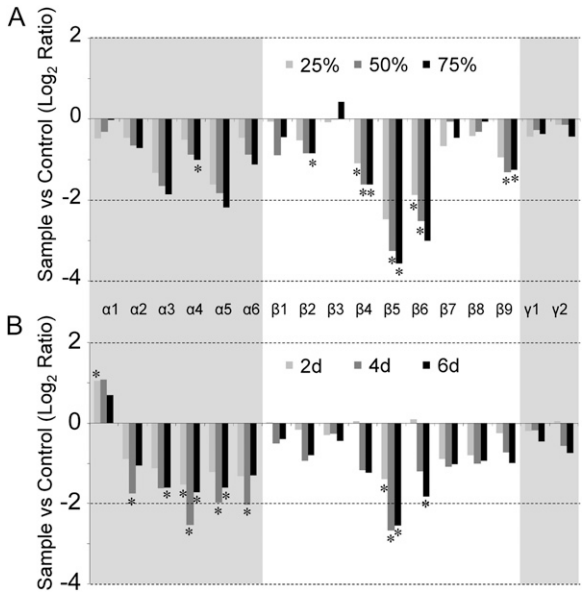

Figure 4. Gene expression analysis of α-, β-, and γ-tubulins during natural senescence (A) and dark-induced senescence (B). Data were primarily extracted from publicly available microarrays (van der Graaff et al., 2006). The normalized expression values were converted into the log2 of the ratio between the samples (25%, 50%, and 75% degradation of chlorophyll) and controls (leaves from 6-week-old plants). Asterisks indicate significant differences ($P < 0.05$) in comparison with the respective T0 determined by Student's *t* test. Samples are as follows: α1 (At1g64740), α2 (At1g50010), α3 (At5g19770), α4 (At1g04820), α5 (At5g19780), α6 (At4g14960), β1 (At1g75780), β2 (At5g62690), β3 (At5g62700), β4 (At5g44340), β5 (At1g20010), β6 (At5g12250), β7 (At2g29550), β8 (At5g23860), β9 (At4g20890), γ1 (At3g61650), γ2 (At5g05620).

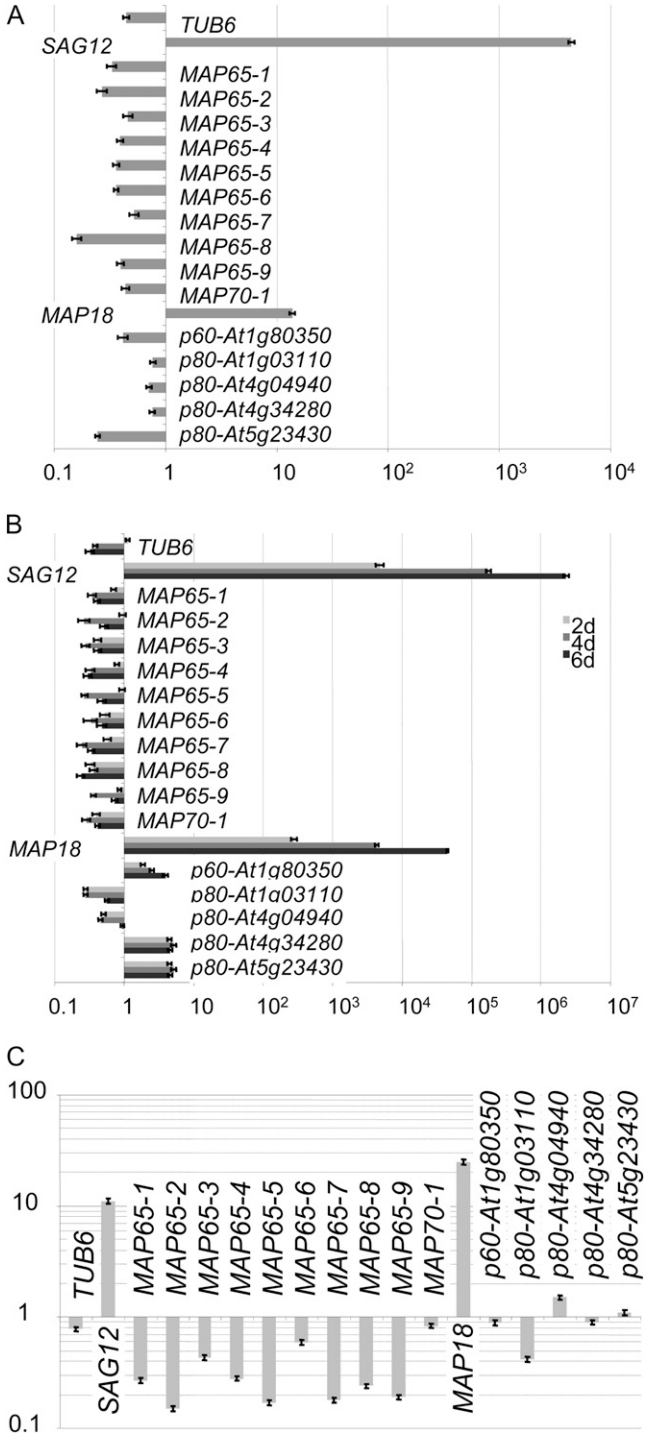

Figure 5. A and B, qRT-PCR analysis of MT-related genes during natural senescence (A) and during dark-induced senescence (B). SAG12 was also included as a molecular marker of leaf senescence. Results are expressed on a $\log_{10}$ scale and represent the ratio between T50ns and T0ns (A) and between T2-idl, T4-idl, or T6-idl and T0-idl (B). C, The ratio between the level of expression of the genes at T0ns and T0idl indicates that senescence has already begun in T0ns. Samples are as follows: TUB6 (At5g12250), MAP18 (At5g44610), MAP65-1 (At5g55230), MAP65-2 (At4g26760), MAP65-3 (At5g51600), MAP65-4 (At3g60840), MAP65-5 (At2g38720), MAP65-6 (At2g01910), MAP65-7 (At1g14690), MAP65-8 (At1g27920), MAP65-9 (At5g62250), MAP70-1 (At1g68060), SAG12 (At5g45890), p60 (At1g80350), p80 (At5g23430), p80 (At1g03110), p80 (At4g34280), p80 (At4g04940).

array. To assess this possibility, we examined by qRT-PCR the level of transcripts of several MT regulators: the nine genes representing the MT-bundling MAP65 family (Smertenko et al., 2008), the MT-severing p60 subunit of katanin (Burk et al., 2001) and four of its putative p80 subunits containing WD40 repeats (Bouquin et al., 2003; Roll-Mecak and McNally, 2010; annotations in TAIR9), the MT-stabilizing MAP70-1 (Korolev et al., 2005), and finally the MT-destabilizing MAP18 (Wang et al., 2007). Results were expressed as the $\log_{10}$ of the ratio between the expression of the genes at T50ns and the expression of the genes at T0ns, for which the expression value was set to 1 (Fig. 5A). Similarly, Figure 5B represents the $\log_{10}$ of the ratio between the gene expression levels at T2idl, T4idl, or T6idl and the expression of the genes at T0idl (for which the value was set to 1). The low abundance of transcripts due to their degradation occurring at T85ns and T8idl did not allow qRT-PCR quantifications.

Often referred to as the main molecular marker of leaf senescence, the level of expression of *SAG12* (for senescence-associated gene 12, encoding a papain-like Cys proteinase) was used as a control and shown to be up-regulated several thousand-fold between T0ns and T50ns and also gradually up-regulated during dark-induced senescence, strengthening the similarities between the two systems. Since the *GFP-TUB6* construct was used for the visualization of the MTs by confocal laser microscopy (Nakamura et al., 2004), we also examined expression of the *TUB6* gene. Reinforcing the validity of the arrays of van der Graaff et al. (2006), we found *TUB6* to be progressively repressed during natural senescence and dark-induced senescence (Fig. 5, A and B).

Due to their central role in plant growth and development, MTs undergo constant reorganization during the different phases of cell expansion and actively participate in intracellular transport and signal transduction in response to hormone signals and/or environmental perturbations. As a direct consequence of their multiple functions, MTs are subjected to extremely complex regulation orchestrated by a plethora of proteins notably involved in building, remodeling, and interconnecting the MT network (Sedbrook, 2004). Among the increasing number of proteins discovered to interact with MTs, we primarily focused on the MAP65 family, as numerous studies have reported MAP65 proteins to be MT-bundling proteins. The Arabidopsis genome contains nine *MAP65* genes sharing 25% to 78% amino acid sequence identity, suggesting an important variability in MAP65 activities (Smertenko et al., 2008). In an effort to unravel the localization and the biochemical roles of the different members of the MAP65 family in Arabidopsis,

Smertenko et al. (2008) provided strong evidence for divergent dynamic association between the MAP65s and the MTs but also highlighted the difficulties of determining in planta the role of each MAP65, due to their tissue and developmental expression specificity. Nonetheless, most of the MAP65 proteins seem to promote MT polymerization at some stage. In this study, we show the expression of all nine *MAP65* genes to be significantly repressed during natural and dark-induced senescence (Fig. 5, A and B). In addition, we also report another *MAP* gene involved in the stabilization of MTs, *MAP70-1* (Korolev et al., 2005), to be down-regulated during the two processes (Fig. 5, A and B).

Interestingly, *MAP18*, whose protein has been demonstrated to have a depolymerizing activity on MTs in vitro (Wang et al., 2007), was found to be highly up-regulated during natural senescence, around 14-fold when compared with T0ns, and also during dark-induced senescence, where its regulation peaked at a 10^4-fold increase, suggesting a major role for MAP18 during leaf senescence. Strong promoter activity of *MAP18* during leaf senescence was confirmed using a promMAP18::GUS reporter gene in transgenic plants (Wang et al., 2007). GUS staining was barely visible in either T0idl or T0ns, but surprisingly, we saw a pronounced staining in structures likely to be the hydathodes of the leaves. Progressively, the GUS staining appeared concomitantly with the progress of the senescence and had a peak of intensity at T4idl and at T50ns (Fig. 6). Although the expression of *promMAP18::GUS* was still detectable in T6idl and T85ns, the staining was not as strong as suggested by the results of the qRT-PCR analysis (Figs. 5 and 6). This discrepancy between the two results may be explained by the fact that the GUS staining reveals only the activity of the promoter of *MAP18*, whereas qRT-PCR reveals the steady-state level of *MAP18* mRNA. Indeed, while the promoter activity is essential to produce *MAP18* mRNAs, the quantity of steady *MAP18* transcripts strongly depends on *MAP18* mRNA stability. From a recently published study on mRNA decay rates in Arabidopsis (Narsai et al., 2007), we discovered that *MAP18* had one of the most stable transcripts in Arabidopsis, with a half-life estimated at 46 h. The group of the most stable transcripts comprises transcripts with a half-life of at least 24 h and represents less than 1% of the 13,000 mRNAs studied (Narsai et al., 2007). The decrease of the *promMAP18* activity in T6idl and the concomitantly high level of *MAP18* mRNAs during senescence are consistent with a particularly high stability of the *MAP18* mRNA in leaves.

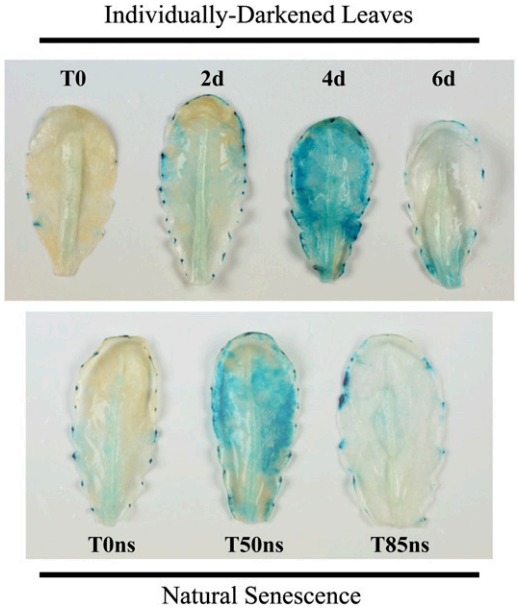

Figure 6. GUS expression analysis of *promMAP18* during dark-induced senescence and natural senescence. Experiments were performed with six independent biological replicates.

Finally, we also investigated the level of expression of katanin subunits. Katanin is a heterodimeric protein that mediates ATP-dependent destabilization of MTs in animals. The small subunit (p60) of katanin has been identified in Arabidopsis and presents a MT-severing activity in vitro, whereas a regulatory subunit of 80 kD (p80) is involved in the targeting of katanin (Stoppin-Mellet et al., 2007). In our work, the p60 subunit of katanin and four of its putative p80 partners were differentially regulated between natural and dark-induced senescence. Whereas the genes coding for the characterized p60 and the four putative p80 subunits were all down-regulated during natural senescence, p60 and two of the four putative p80 subunits appeared to be significantly up-regulated during dark-induced senescence. This discrepancy between natural and dark-induced senescence suggests katanin to be somehow regulated by light.

Whole Darkened Plants as a Control

In an attempt to dissociate the effects of darkness from the process of cell death occurring in leaves subjected to dark-induced senescence, we examined the expression level of the same set of genes in leaves harvested after 2, 4, and 6 d from entirely darkened plants. We previously showed (Keech et al., 2007) that after 6 d of darkness, leaves from entirely darkened plants were in a metabolic "standby" mode, where most of the cellular functions were reduced but still kept functional in order to optimize the recovery of the plant when a source of light became available. While idls are inexorably committed to senesce, this fundamentally different metabolic strategy confers to the entirely darkened plant a crucial survival ability. The qRT-PCR analysis revealed an intermediate transcript profile in the leaves from the entirely darkened plants. As in idls, *MAP18*, *p60-At1g80350*, *p80-At4g34280*, and *p80-At5g23430* were progressively up-regulated during the 6 d of darkness. However, idls and whole

darkened plants differed, as *TUB6* was significantly up-regulated and all genes encoding MAP65 and MAP70-1 were stably expressed (Fig. 7A). Interestingly, only a minor reduction of the density of the MT network was observed in leaves from 6-d-darkened plants (Fig. 7B).

DISCUSSION

Both Natural and Dark-Induced Senescence Are Accompanied by an Early, Cell-Specific Degradation of the Cortical MT Array

Although leaf senescence is a thoroughly studied developmental stage, the role of the cytoskeleton remains unknown. Consequently, our objective in this study was to characterize the cortical MT array during leaf senescence and to investigate its potential regulation. Natural senescence is the obvious physiological reference for studies about leaf senescence. However, working with different experimental systems can sometimes be advantageous because the comparison of the results unravels common or specific pathways and also helps to establish more accurately the interconnections between pathways leading to leaf senescence. In this study, despite T0ns being 4 weeks older than T0idl, no visible sign of senescence was apparent. Indeed, no degradation of chlorophyll was evident (the chlorophyll content was even 30% higher in T0ns than in T0-idl), the immunoblot analysis of Rubisco and of α-tubulin revealed a high amount of protein in the two T0s, and finally, the comparison of the MT cytoskeleton between the two did not show apparent differences. However, for a few genes of interest, the ratios between the expression levels in T0ns and in T0idl demonstrate that the T0ns leaves may have already entered the process of senescence (Fig. 5C). For instance, the high expression of *SAG12* clearly indicates that the genetically controlled process of degradation has already begun in T0ns (Fig. 5C). In addition, it has been shown that in leaves under normal conditions, the chloroplastic isoform (GS2) represents the main fraction of the Gln synthetase pool, while the cytosolic isoform (GS1) is more abundant during leaf senescence (Kawakami and Watanabe, 1988; Brugière et al., 2000; Masclaux et al., 2000). The higher protein ratio of GS1 to GS2 in T0ns leaves when compared with T0idl indicates that these leaves have already modified their metabolism to enter their nutrient recycling process and in particular the salvage of nitrogen. In addition, as shown by Supplemental Figure S1, leaves undergoing natural senescence exhibit a more heterogeneous degradation pattern than leaves subjected to a dark-induced senescence. Taken together, these results show the difficulties in determining the starting point of natural senescence without using destructive techniques. For this reason, the use of other systems such as dark-induced senescence, which allows a fast, controlled, and more synchronous induction of leaf senescence, appears to be a powerful tool to study leaf senescence.

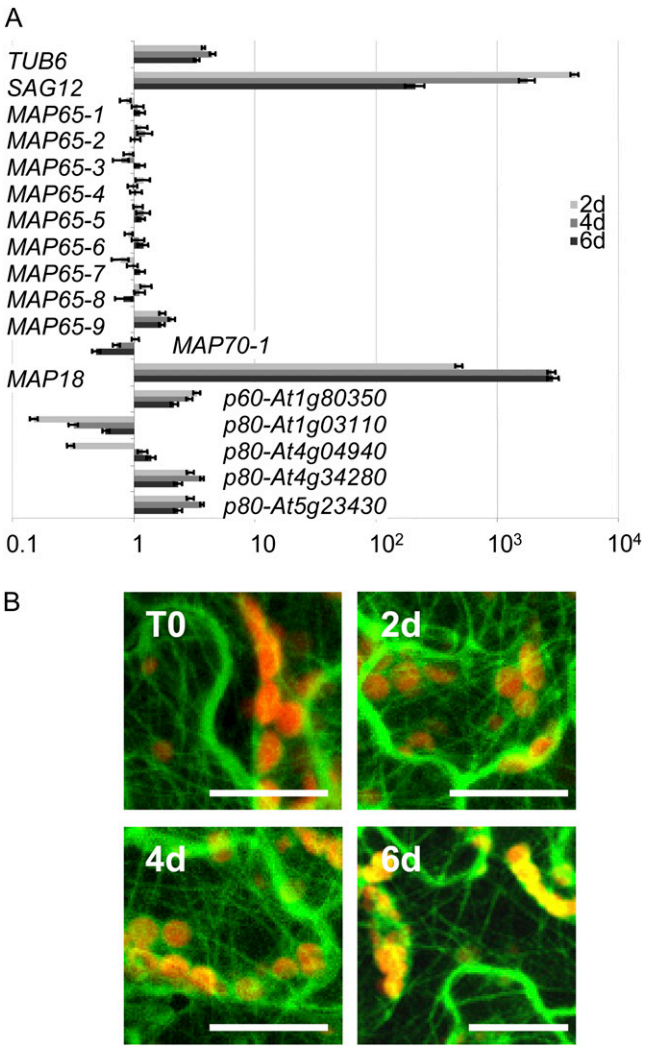

Figure 7. A, qRT-PCR analysis of MT-related genes in leaves from entirely darkened plants. Results are expressed on a $\log_{10}$ scale and represent the ratio between 2 d, 4 d, or 6 d and T0. All locus identifiers are available in the legend of Figure 5. B, In folio imaging of the MT array during 0, 2, 4, and 6 d in darkness. Bars = 20 μm.

Here, we show that the degradation of the cortical MT array is an early event and takes place in the epidermis cells and the adjacent layer of mesophyll cells of Arabidopsis leaves undergoing either natural or dark-induced senescence (Figs. 2 and 3). Only a minor aggregation of the chloroplasts in mesophyll cells from both natural and dark-induced leaf senescence is observed, whereas such aggregation was more apparent in a previous study (Keech et al., 2007). However as infiltrations of calcofluor white were used to visualize the cell wall in our previous study (Keech et al., 2007), this might have accentuated the aggregation of the organelles, since they could not be properly anchored to the cytoskeleton due to its destabilization. In contrast, guard cells of stomata conserve their

chloroplasts and their MT network, consistent with earlier studies reporting the extended longevity of chloroplasts from guard cells of yellowing leaves from both perennial and annual plants (Zeiger and Schwartz, 1982). It has been proposed that guard cells of stomata retain their functionalities to facilitate gas exchanges until the very end of the senescence process (Thimann and Satler, 1979). However, the heterogeneity in the metabolism of the different cell types during leaf senescence raises fundamental questions about cell-specific regulation and potential signaling between the cells undergoing senescence.

Molecular Mechanisms of the Degradation of the MT Arrays during Leaf Senescence

Smertenko et al. (2003) have reported disorganization of the MTs during embryonic programmed cell death in the gymnosperm *Picea abies*, and degradation of the MTs was also observed by Zottini et al. (2006) in cytokinin-treated cells of *Medicago truncatula* induced to enter programmed cell death. However, the molecular players and the regulatory mechanisms responsible for this destabilization remain unknown.

We assume that although MT assembly is energy dependent, the lack of ATP/GTP is not likely to be responsible for the disorganization of the MT, as we earlier showed mitochondria to provide sufficient ATP to maintain cellular functions until the end of the process of senescence (Keskitalo et al., 2005; Keech et al., 2007). So, in an attempt to elucidate the molecular mechanisms responsible for the degradation of the MT lattice during leaf senescence, we investigated the regulation of genes coding for tubulin subunits and for several MAPs in whole leaves. Expression of genes encoding α-, β-, and γ-tubulins is mainly repressed during leaf senescence, as shown by published microarray data (van der Graaff et al., 2006). In addition, we show that the *MAP65* gene family and *MAP70-1* are significantly repressed during both natural and dark-induced senescence but not in leaves from whole plants experiencing prolonged darkness. This consequently suggests that MT polymerization and stabilization mechanisms are specifically downregulated during leaf senescence.

However, not all MAPs are involved in the stabilization of MTs. Recently identified as a new MAP (Wang et al., 2007), MAP18 was shown to bind to MTs and to inhibit tubulin polymerization in vitro. *MAP18* was reported to be expressed mostly in expanding cells and localized in root, flower, cotyledon, hypocotyl, and trichome but surprisingly not in the root tip or mature leaf (Wang et al., 2007). Using the *GUS* reporter gene fused to the promoter of *MAP18*, we observed a specific staining of structures believed to be hydathodes of mature leaves under normal conditions (T0ns and T0idl). However, both qRT-PCR and GUS staining showed an increased expression of *MAP18* during leaf senescence, strongly supporting the idea that MAP18 could play a physiological role in the senescence-specific degradation of MTs. However, our analysis showed that *MAP18* was also induced in leaves from whole darkened plants, whereas only a minor destabilization of the MT network was observed. Furthermore, in a recent study, Kato et al. (2010) investigated the biochemical properties of MAP18 and concluded that this protein was a plasma membrane-associated Ca^{2+}-binding protein (consequently renamed PCaP2 by the authors) and was very likely to be involved in the regulation of cellular functions, including stress response and cytoskeletal reorganization. In vivo, MAP18/PCaP2 appeared to be associated with the plasma membrane due to its *N*-myristoylation and strongly interacted with several phosphatidylinositol phosphates in a Ca^{2+}-calmodulin-dependent manner (Kato et al., 2010). We consequently conclude that increased expression of *MAP18* is not sufficient to destabilize the MT network in vivo but could instead be part of a more complex Ca^{2+}-dependent signaling mechanism potentially leading to the perturbation of the MT cytoskeleton.

We also questioned whether katanin could be involved in the degradation of MTs. In a recent study, Stoppin-Mellet et al. (2006) examined in Arabidopsis the overexpression of the p60 subunit (also called AtKSS or AtKTN1) fused to the reporter monomeric Red Fluorescent Protein. Under the control of an ethanol-inducible promoter, overexpression of the katanin p60 subunit triggered MTs to organize into numerous and thick bundles, which ultimately depolymerized. In this work, our findings showed that all

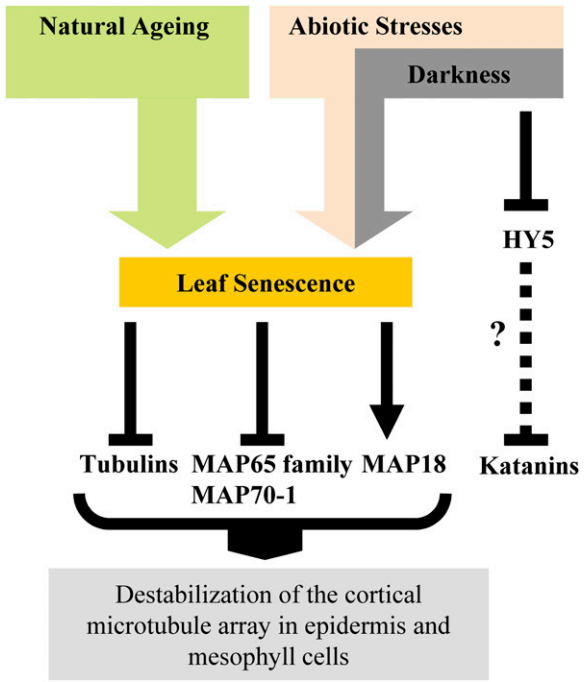

Figure 8. Proposed model for the destabilization of the cortical MT array in epidermis and mesophyll cells during leaf senescence. [See online article for color version of this figure.]

katanin subunit genes (i.e. the *p60* and putative *p80* genes) were all repressed during natural senescence, whereas the genes encoding *p60* and two of the putative *p80* genes were significantly up-regulated in idls (Fig. 5, A and B). Despite this up-regulation during dark-induced senescence, the formation of short and thick bundles was not apparent. Consequently, katanin does not seem to be required for the depolymerization of MTs during leaf senescence. However, the discrepancy between the data from natural senescence and from dark-induced senescence suggests that the severing activity of katanin could be involved in the rearrangement of MT in a light-dependent manner. In fact, this idea is further supported by the two following points. First, qRT-PCR performed on leaves from entirely darkened plants revealed the same *p60* and *p80* transcripts to be significantly up-regulated during 6 d of darkness (Fig. 7A), although only a minor degradation of the cortical MT array was noticed (Fig. 7B). Second, when we examined the ChIP-chip data set from Lee et al. (2007), we observed that *AtKSS* (p60-At1g80350) was among the in vivo binding targets of the transcription factor HY5 (for long hypocotyl 5). The bZIP protein HY5 is an extensively studied transcription factor involved in promoting photomorphogenesis. Mutations in *HY5* cause a defect in the inhibition of hypocotyl elongation in all light conditions, suggesting that HY5 acts downstream of PHYA, PHYB, cryptochromes, and UV-B light (Lee et al., 2007). Taken together, these results strongly suggest that the severing activity of katanin on the remodeling of the cortical MT array can be light dependent, since darkness on the one hand enhances katanin expression and on the other hand represses the expression of *HY5*. However, much work remains to elucidate the regulation of the cortical MTs in response to developmental and environmental stimuli.

To conclude, in view of these new findings, we propose a tentative model (Fig. 8) for the early degradation of the cortical MT lattice during both natural and dark-induced senescence. Katanin p60 and p80 subunits may not be required during natural senescence; however, they could contribute to the reorganization and the severing of the MTs during prolonged darkness, including dark-induced senescence, potentially via the repression of the transcription factor HY5. In contrast, the corepression of the tubulin subunits and the bundling/stabilizing MAP65s/MAP70-1 could contribute to the destabilization of the MT network during leaf senescence; the minor disruption of the MTs observed in leaves from entirely darkened plants suggests that *MAP18* expression alone is not sufficient for the disruption of the MTs. Altogether, this work highlights a novel trait of leaf senescence by demonstrating the surprising earliness of the degradation of the cortical MT array. This also leads to further questions about how vesicle shuttling, organelle mobility, and reorganization of metabolism are achieved in cells having a drastically reduced MT network.

MATERIALS AND METHODS

Plant Material and Growth Conditions

Arabidopsis (*Arabidopsis thaliana*) ecotype Columbia and Columbia transformed with GFP-TUB6 (Nakamura et al., 2004; Abe and Hashimoto, 2005) were grown in a controlled-environment growth chamber with a short-day photoperiod (8 h of light/16 h of dark), an irradiance of 250 μmol quanta m^{-2} s^{-1}, a relative humidity of 75%, and a temperature cycle of 22°C day/17°C night.

Induction of Senescence

Leaves undergoing natural senescence were collected from rosettes (leaves 6–11) from plants aged 11 to 13 weeks. The three stages were labeled T0ns, T50ns, and T85ns. T0ns represented leaves with a chlorophyll content of 2.2 ± 0.4 mg mL^{-1} g^{-1} fresh weight. T50ns and T85ns were, respectively, the leaves undergoing natural senescence with 50% and more than 85% degradation of their chlorophyll content.

Dark-induced senescence was carried out as described by Keech et al. (2007). Briefly, with Arabidopsis plants aged 8 weeks, rosette leaves 6 to 11 were covered by mittens for 2, 4, 6, and 8 d while the rest of the plant remained in the light. These leaves are referred to as idls. In parallel, whole plants were placed in darkness for 2, 4, and 6 d.

Protein Extraction and Immunoblot Analysis

For each treatment, two leaf discs (diameter 15 mm) were ground in 500 μL of extraction buffer (50 mM Tris-HCl, pH 7.5, 5 mM EGTA, 5 mM $MgCl_2$, 100 mM NaCl, 10% [v/v] glycerol, 0.1% [v/v] Triton-X-100, 0.5% [w/v] SDS, and 2 mM dithiothreitol). After centrifugation (4°C, 15 min, 20,000*g*), supernatants were collected and protein amount was quantified with the DC Protein Assay Kit from Bio-Rad.

Immunoblot analysis was done on nitrocellulose, and primary antibodies were used at the following concentrations: anti-large subunit of Rubisco (from Agrisera), 1:5,000; anti-COX-II (from Agrisera), 1:1,000; anti-GS1 and anti-GS2 (Sakakibara et al., 1992), 1:1,000; anti-TUBα (from Sigma; T5168), 1:2,000; anti-Actin (from Sigma; A0480), 1:1,000. Western blots were visualized by enhanced chemiluminescence (GE Healthcare).

Confocal Laser Imaging: MT Network Visualization

Imaging was performed with an SP2 inverted microscope (Leica) under a 63× water-immersion objective (numerical aperture 1.20). The MT cytoskeleton was visualized in the epidermis and the adjacent layer of spongy mesophyll cells from the abaxial side of the leaf sections. GFP was excited using a 488-nm silver laser, and emitted light was collected in the 503- to 562-nm window. Chloroplasts revealed by chlorophyll fluorescence were excited using a 633-nm helium-neon laser, and emitted light was collected in the 662- to 721-nm window. Spectral measurements were performed to confirm emission spectra. Three-dimensional images of leaves were made by sequential scans. For each time point, at least four biological replicates were processed. Images were mounted with the ImageJ software (version1.38x).

Transcript Quantification by qRT-PCR

RNA Isolation and cDNA Synthesis

Ten leaves at similar stages of senescence (i.e. T0ns and T50ns for natural senescence and T0, 2 d, 4 d, and 6 d for idl and whole darkened plants [see above for description]) were dissected from five different plants, pooled, frozen in liquid nitrogen, and ground into powder. Two sets of samples were prepared from two independent biological replicates. Total RNA was extracted using the hot phenol protocol described by Gutierrez et al. (2008). The resulting RNA preparations were treated with DNaseI using the DNAfree Kit (Ambion), and cDNA was synthesized by reverse transcribing 10 μg of total RNA using SuperScript II reverse transcriptase (Invitrogen) according to the manufacturer's instructions. The reaction was stopped by incubation at 70°C for 10 min, and the reaction mixture was then treated with RNaseH (Invitrogen) according to the manufacturer's instructions and diluted by adding 700 μL of deionized water. All cDNA samples were tested by PCR using specific primers flanking an intron sequence to confirm the absence of genomic DNA contamination.

qRT-PCR

Transcript levels were assessed by qRT-PCR in assays with triplicate reaction mixtures (final volume, 20 μL) containing 5 μL of cDNA, 0.5 μM of both forward and reverse primers, and 1× FastStart SYBR Green Master Mix (Roche) using an iCycler iQ Real-Time PCR Detection System (Bio-Rad), and threshold cycle (CT) values for each sample were acquired using iCycler iQ software 3.0 (Bio-Rad). The following standard protocol was applied for each amplification: 10 min at 95°C, followed by 40 cycles of 10 s at 95°C, 15 s at 60°C, and 15 s at 72°C. The sequences of primers used for all target genes are presented in Supplemental Table S1.

Reference genes were selected and validated as follows. Ten genes (for primer sequences, see Supplemental Table S2) were chosen for their putative stability of expression according to Czechowski et al. (2005) and Gutierrez et al. (2008). Their expression in our experimental material (i.e. leaves at different stages of natural or artificial senescence grown under our experimental conditions) was then assessed, and they were ranked according to their stability of expression using the geNorm software (Vandesompele et al., 2002). *APT1* and *TIP41* were the most stably expressed genes among the 10 tested (Supplemental Fig. S2) and thus were used to normalize the qRT-PCR data. The normalized expression patterns obtained using both reference genes were similar, so only the data normalized with *APT1* are shown in Figures 4, 5, and 7. Relative standard curves describing the PCR efficiencies for each primer pair were generated for each amplicon, and the resulting values were used to calculate expression using the formula $E_T^{(CT_{T0} - CT_X)}/E_R^{(CT_{T0} - CT_X)}$, where T is the target gene and R is the reference gene, CT is the crossing threshold value (i.e. the number of PCR cycles required for the accumulated fluorescence signal to cross a threshold above the background), X is related to cDNA from senescing leaves (i.e. T2idl, T4idl, T6idl, and T50ns), and T0 indicates the related T0 control (i.e. T0ns and T0idl). A melting curve analysis was added to each PCR program, and the size of PCR products was assessed by electrophoresis on agarose gels to check that the fluorescence signal was derived from the single intended amplicon.

promMAP18::GUS Analysis

Stable transformants for promMAP18::GUS (in the Columbia background) were kindly obtained from Prof. Ming Yuan. GUS staining was performed according to Wang et al. (2007).

Supplemental Data

The following materials are available in the online version of this article.

Supplemental Figure S1. Example of heterogeneity in the degradation of the MT network during natural leaf senescence.

Supplemental Figure S2. Validation of the reference genes (geNorm) for the qRT-PCR analysis.

Supplemental Table S1. Sequences of primers used for target genes.

Supplemental Table S2. Sequences of primers used for reference genes.

Supplemental Table S3. Relative expression values for natural and dark-induced senescence time courses.

ACKNOWLEDGMENTS

We thank Dr. Hitoshi Sakakibara for GS1 and GS2 antibodies, Dr. Akashi Hashimoto for the transgenic Arabidopsis line GFP-TUB6, and Prof. Ming Yuan for the promMAP18::GUS line. Dr. Andreas Sjödin is acknowledged for his comments at the early stages of this work.

Received July 25, 2010; accepted October 18, 2010; published October 21, 2010.

LITERATURE CITED

Abe T, Hashimoto T (2005) Altered microtubule dynamics by expression of modified alpha-tubulin protein causes right-handed helical growth in transgenic Arabidopsis plants. Plant J **43:** 191–204

Bouquin T, Mattsson O, Naested H, Foster R, Mundy J (2003) The Arabidopsis lue1 mutant defines a katanin p60 ortholog involved in hormonal control of microtubule orientation during cell growth. J Cell Sci **116:** 791–801

Boutté Y, Vernhettes S, Satiat-Jeunemaitre B (2007) Involvement of the cytoskeleton in the secretory pathway and plasma membrane organisation of higher plant cells. Cell Biol Int **31:** 649–654

Brugière N, Dubois F, Masclaux C, Sangwan RS, Hirel B (2000) Immunolocalization of glutamine synthetase in senescing tobacco (*Nicotiana tabacum* L.) leaves suggests that ammonia assimilation is progressively shifted to the mesophyll cytosol. Planta **211:** 519–527

Burk DH, Liu B, Zhong R, Morrison WH, Ye Z-H (2001) A katanin-like protein regulates normal cell wall biosynthesis and cell elongation. Plant Cell **13:** 807–827

Czechowski T, Stitt M, Altmann T, Udvardi MK, Scheible W-R (2005) Genome-wide identification and testing of superior reference genes for transcript normalization in Arabidopsis. Plant Physiol **139:** 5–17

Dixit R, Cyr R (2004) The cortical microtubule array: from dynamics to organization. Plant Cell **16:** 2546–2552

Gutierrez L, Mauriat M, Guénin S, Pelloux J, Lefebvre JF, Louvet R, Rusterucci C, Moritz T, Guerineau F, Bellini C, et al (2008) The lack of a systematic validation of reference genes: a serious pitfall undervalued in reverse transcription-polymerase chain reaction (RT-PCR) analysis in plants. Plant Biotechnol J **6:** 609–618

Hamada T (2007) Microtubule-associated proteins in higher plants. J Plant Res **120:** 79–98

Hashimoto T (2003) Dynamics and regulation of plant interphase microtubules: a comparative view. Curr Opin Plant Biol **6:** 568–576

Hashimoto T, Kato T (2006) Cortical control of plant microtubules. Curr Opin Plant Biol **9:** 5–11

Kato M, Nagasaki-Takeuchi N, Ide Y, Maeshima M (2010) An Arabidopsis hydrophilic Ca2(+)-binding protein with a PEVK-rich domain, PCaP2, is associated with the plasma membrane and interacts with calmodulin and phosphatidylinositol phosphates. Plant Cell Physiol **51:** 366–379

Kawakami N, Watanabe A (1988) Senescence-specific increase in cytosolic glutamine synthetase and its mRNA in radish cotyledons. Plant Physiol **88:** 1430–1434

Keech O, Pesquet E, Ahad A, Askne A, Nordvall DAG, Vodnala SM, Tuominen H, Hurry V, Dizengremel P, Gardeström P (2007) The different fates of mitochondria and chloroplasts during dark-induced senescence in Arabidopsis leaves. Plant Cell Environ **30:** 1523–1534

Keskitalo J, Bergquist G, Gardeström P, Jansson S (2005) A cellular timetable of autumn senescence. Plant Physiol **139:** 1635–1648

Kopczak SD, Haas NA, Hussey PJ, Silflow CD, Snustad DP (1992) The small genome of *Arabidopsis* contains at least six expressed α-tubulin genes. Plant Cell **4:** 539–547

Korolev AV, Chan J, Naldrett MJ, Doonan JH, Lloyd CW (2005) Identification of a novel family of 70 kDa microtubule-associated proteins in Arabidopsis cells. Plant J **42:** 547–555

Lee J, He K, Stolc V, Lee H, Figueroa P, Gao Y, Tongprasit W, Zhao H, Lee I, Deng XW (2007) Analysis of transcription factor HY5 genomic binding sites revealed its hierarchical role in light regulation of development. Plant Cell **19:** 731–749

Liu B, Joshi HC, Wilson TJ, Silflow CD, Palevitz BA, Snustad DP (1994) γ-Tubulin in *Arabidopsis*: gene sequence, immunoblot, and immunofluorescence studies. Plant Cell **6:** 303–314

Lloyd C (2006) Plant science: Microtubules make tracks for cellulose. Science **312:** 1482–1483

Lloyd C, Hussey P (2001) Microtubule-associated proteins in plants: why we need a MAP. Nat Rev Mol Cell Biol **2:** 40–47

Masclaux C, Valadier MH, Brugière N, Morot-Gaudry JF, Hirel B (2000) Characterization of the sink/source transition in tobacco (Nicotiana tabacum L.) shoots in relation to nitrogen management and leaf senescence. Planta **211:** 510–518

Nakamura M, Naoi K, Shoji T, Hashimoto T (2004) Low concentrations of propyzamide and oryzalin alter microtubule dynamics in Arabidopsis epidermal cells. Plant Cell Physiol **45:** 1330–1334

Narsai R, Howell KA, Millar AH, O'Toole N, Small I, Whelan J (2007) Genome-wide analysis of mRNA decay rates and their determinants in *Arabidopsis thaliana*. Plant Cell **19:** 3418–3436

Nooden LD, Guiamet JJ, John I (1997) Senescence mechanisms. Physiol Plant **101:** 746–753

Pesquet E, Korolev AV, Calder G, Lloyd CW (2010) The microtubule-

associated protein AtMAP70-5 regulates secondary wall patterning in Arabidopsis wood cells. Curr Biol **20:** 744–749

Roll-Mecak A, McNally FJ (2010) Microtubule-severing enzymes. Curr Opin Cell Biol **22:** 96–103

Romagnoli S, Cai G, Faleri C, Yokota E, Shimmen T, Cresti M (2007) Microtubule- and actin filament-dependent motors are distributed on pollen tube mitochondria and contribute differently to their movement. Plant Cell Physiol **48:** 345–361

Sakakibara H, Kawabata S, Takahashi H, Hase T, Sugiyama T (1992) Molecular cloning of the family of glutamine synthetase genes from maize: expression of genes for glutamine synthetase and ferredoxin-dependent glutamate synthase in photosynthetic and non-photosynthetic tissues. Plant Cell Physiol **33:** 49–58

Sedbrook JC (2004) MAPs in plant cells: delineating microtubule growth dynamics and organization. Curr Opin Plant Biol **7:** 632–640

Smart C (1994) Gene expression during leaf senescence. New Phytol **126:** 419–448

Smertenko AP, Bozhkov PV, Filonova LH, von Arnold S, Hussey PJ (2003) Re-organisation of the cytoskeleton during developmental programmed cell death in Picea abies embryos. Plant J **33:** 813–824

Smertenko AP, Kaloriti D, Chang HY, Fiserova J, Opatrny Z, Hussey PJ (2008) The C-terminal variable region specifies the dynamic properties of *Arabidopsis* microtubule-associated protein MAP65 isotypes. Plant Cell **20:** 3346–3358

Snustad DP, Haas NA, Kopczak SD, Silflow CD (1992) The small genome of *Arabidopsis* contains at least nine expressed beta-tubulin genes. Plant Cell **4:** 549–556

Stoppin-Mellet V, Gaillard J, Timmers T, Neumann E, Conway J, Vantard M (2007) Arabidopsis katanin binds microtubules using a multimeric microtubule-binding domain. Plant Physiol Biochem **45:** 867–877

Stoppin-Mellet V, Gaillard J, Vantard M (2006) Katanin's severing activity favors bundling of cortical microtubules in plants. Plant J **46:** 1009–1017

Thimann KV, Satler SO (1979) Relation between leaf senescence and stomatal closure: senescence in light. Proc Natl Acad Sci USA **76:** 2295–2298

van der Graaff E, Schwacke R, Schneider A, Desimone M, Flügge UI, Kunze R (2006) Transcription analysis of Arabidopsis membrane transporters and hormone pathways during developmental and induced leaf senescence. Plant Physiol **141:** 776–792

Vandesompele J, De Preter K, Pattyn F, Poppe B, Van Roy N, De Paepe A, Speleman F (2002) Accurate normalization of real-time quantitative RT-PCR data by geometric averaging of multiple internal control genes. Genome Biol **3:** research0034

Van Gestel K, Köhler RH, Verbelen JP (2002) Plant mitochondria move on F-actin, but their positioning in the cortical cytoplasm depends on both F-actin and microtubules. J Exp Bot **53:** 659–667

Wada M, Suetsugu N (2004) Plant organelle positioning. Curr Opin Plant Biol **7:** 626–631

Wang X, Zhu L, Liu B, Wang C, Jin L, Zhao Q, Yuan M (2007) *Arabidopsis* MICROTUBULE-ASSOCIATED PROTEIN18 functions in directional cell growth by destabilizing cortical microtubules. Plant Cell **19:** 877–889

Wasteneys GO (2004) Progress in understanding the role of microtubules in plant cells. Curr Opin Plant Biol **7:** 651–660

Weaver LM, Amasino RM (2001) Senescence is induced in individually darkened Arabidopsis leaves, but inhibited in whole darkened plants. Plant Physiol **127:** 876–886

Wightman R, Turner SR (2008) The roles of the cytoskeleton during cellulose deposition at the secondary cell wall. Plant J **54:** 794–805

Woolhouse H (1967) The nature of senescence in plants. *In* H Woolhouse, ed, Aspects of the Biology of Aging, Vol XXI. Cambridge University Press, Cambridge, UK, pp 179–213

Yoshida S (2003) Molecular regulation of leaf senescence. Curr Opin Plant Biol **6:** 79–84

Zeiger E, Schwartz A (1982) Longevity of guard cell chloroplasts in falling leaves: implication for stomatal function and cellular aging. Science **218:** 680–682

Zottini M, Barizza E, Bastianelli F, Carimi F, Lo Schiavo F (2006) Growth and senescence of Medicago truncatula cultured cells are associated with characteristic mitochondrial morphology. New Phytol **172:** 239–247

Supplementary Table 1: Sequences of primers used for quantifying target genes by quantitative RT-PCR

Gene family	Common name	Locus	Forward Primer	Reverse Primer
TUBULIN	β-TUBULIN 6	At5g12250	GAGAGACCTCGGGGAGCTAT	TGGCAAGATGAGCACAAAAG
MAP	MAP18	At5g44610	TGGCTGAAACTCCTTCGACT	GAAAATTCAAGCCTTTTGTGG
MAP	MAP65-1	At5g55230	TGAATGCAAACCAGAATGGA	TGATCTGCAGCACCAGAAAC
MAP	MAP65-2	At4g26760	ACGGAAGCAAGTCCAAGAGA	TCAGCACGAGAGACTGGAGA
MAP	MAP65-3	At5g51600	CCATTCACCAACAATGCAAG	TGAATCCAACGGATTGATGA
MAP	MAP65-4	At3g60840	CTGCAGCTTCAGTCGCTATG	GCCCTAACCTCTTCAAACGA
MAP	MAP65-5	At2g38720	GAAGAAGCCATTGGGACAGA	TCACCGCATTGCCTCTATAA
MAP	MAP65-6	At2g01910	GGCCATGCAAAAGGAAGATA	CGGTGGAAAAGAGAGTCAAG
MAP	MAP65-7	At1g14690	ACCGAGTCCAAGAAGAAGCA	GGCGATGGCTTGAGTATGAT
MAP	MAP65-8	At1g27920	GATGAGCATTCCACAACCTG	TCCACTTCCAAATCCACCAT
MAP	MAP65-9	At5g62250	AAGTGTTACGAAGCCCCAAA	CCATGGCGTGATAGAGGAGT
MAP	MAP70-1	At1g68060	CACACCAGCCTATAACGGTTT	CCGAAGTGGGTTAACAAGGA
Cysteine-protease	SAG12	At5g45890	AAAGGCGAAGACGCTACTTG	CCTTCATCAGTGCTTGCTCA
Katanin	p60 katanin	At1g80350	TCAGGAGGAGGTTGGAAAAA	TCCACTGTACCCTTCCGTTC
WD-40 repeat family protein	p80 katanin	At5g23430	GAGCCATTGGGCTGTGTATT	CCGCGAAAAACCTCTATTCA
WD-40 repeat family protein	p80 katanin	At1g03110	GGGACCAAACTATTGGAGCA	ATCAAAAGGCTGGACATTGC
WD-40 repeat family protein	p80 katanin	At4g34280	GTGATCCGTGTTTGTTGTGC	CACCGCGTAGAGACTGAACA
WD-40 repeat family protein	p80 katanin	At4g04940	GCCCGCAATAAACCAATAGA	TTCCTCATTCTCCCCATCAG

Supplementary Table 2: Sequences of primers for putative reference genes tested by geNorm

Gene name	Forward primer	Reverse primer
eF1α - At5g60390	TGGTGACGCTGGTATGGTTA	TCCTTCTTGTCCACGCTCTT
APT1 - At1g27450	GAGACATTTTGCGTGGGATT	CGGGGATTTTAAGTGGAACA
UBQ5 - At3g62250	CCAAGCCGAAGAAGATCAAG	ACTCCTTCCTCAAACGCTGA
SAND family protein - At2g28390	GGGGGTCAAACCAGTAGAAA	ATCAGGTGTGCCAAAGGGTA
TIP41-like family protein At4g34270	GCTCATCGGTACGCTCTTTT	TCCATCAGTCAGAGGCTTCC
At4g26410	TTTCCAATTGAATCGCAGTG	AGGAAGCAGGCAAAAACACA
At4g33380	GTGTTGTAACGGCTTGAGCA	TGTTTGCATCTTTGGTACGG
Clathrin adaptor complexes medium subunit family protein At5g46630	GTTTGGGAGAAGAGCGGTTA	CTGATGTCACTGAACCTGAACTG
PPR repeat-containing protein At5g55840	GCAAGACAGTGAAGGTGCAA	CAGCGTTTATCAACCCACCT
GAPC-2 - At1g13440	CGCATGGAATCAGTGAAAAA	TCGTGTCGTTGACCTTATCG

Supplemental table 3. Relative expression values for natural senescence (a) and dark-induced senescence (b) time courses extracted from suppl. data van der Graaff (2006). t-test comparisons were performed and p-values<0.05 were considered as significant. Fold-change is also included.

a

Name	Locus	NS1_6w	NS2_6w	NS1_25	NS2_25	NS1_50	NS2_50	NS1_75	NS2_75	p-value (T0-25)	p-value (T0-50)	p-value (T0-75)	fold (T0-25)	fold (T0-50)	fold (T0-75)
tubulin alpha-1 chain (TUA1)	At1g64740	5489	3912	3622	3096	3661	3899	3799	5463	0.2479	0.3677	0.9572	-1.4	-1.2	-1.0
tubulin alpha-2/alpha-4 chain (TUA2)	At1g50010	5404	9556	4949	5885	5016	4493	3942	5121	0.4346	0.3225	0.3052	-1.4	-1.6	-1.7
tubulin alpha-3/alpha-5 chain (TUA3)	At5g19770	16789	35201	11847	8858	9660	6918	7997	6385	0.2355	0.1975	0.1788	-2.5	-3.1	-3.6
tubulin alpha-2/alpha-4 chain (TUA4)	At1g04820	11212	14001	8849	8900	7768	5892	6628	5965	0.1159	0.0752	0.0479	-1.4	-1.8	-2.0
tubulin alpha-3/alpha-5 chain (TUA5)	At5g19780	11289	31664	8213	5747	7777	4280	5689	3722	0.2933	0.2736	0.2430	-3.1	-3.6	-4.6
tubulin alpha-6 chain (TUA6)	At4g14960	23614	42211	23429	24380	19364	16338	14649	15759	0.4354	0.2510	0.1977	-1.4	-1.8	-2.2
tubulin beta-1 chain (TUB1)	At1g75780	93	182	168	98	61	88	50	153	0.9439	0.3082	0.6497	-1.0	-1.8	-1.4
tubulin beta-2/beta-3 chain (TUB2)	At5g62690	17856	16167	16043	7592	11966	6922	9838	9009	0.3513	0.1045	0.0150	-1.4	-1.8	-1.8
tubulin beta-2/beta-3 chain (TUB3)	At5g62700	414	458	507	318	474	392	470	703	0.8312	0.9545	0.3320	-1.1	-1.0	1.3
tubulin beta-4 chain (TUB4)	At5g44340	14565	17022	8471	6417	5873	4416	5448	4836	0.0349	0.0175	0.0138	-2.1	-3.1	-3.1
tubulin beta-5 chain (TUB5)	At1g20010	2625	3963	804	383	411	277	225	334	0.0613	0.0482	0.0462	-5.6	-9.6	-11.8
tubulin beta-6 chain (TUB6)	At5g12250	2802	3575	1055	681	688	420	389	409	0.0326	0.0233	0.0187	-3.7	-5.8	-8.0
tubulin beta-7 chain (TUB7)	At2g29550	653	742	382	493	311	1032	350	663	0.0674	0.9495	0.3613	-1.6	-1.0	-1.4
tubulin beta-8 chain (TUB8) (TUBB8)	At5g23860	9159	15740	9810	8954	8696	11252	7878	15949	0.4528	0.5557	0.9274	-1.3	-1.2	-1.0
tubulin beta-9 chain (TUB9)	At4g20890	7939	8786	5360	3363	3978	2786	3725	3338	0.0663	0.0209	0.0092	-1.9	-2.5	-2.4
tubulin gamma-1 chain / gamma-1 tubulin (TUBG1)	At3g61650	590	454	392	380	322	548	351	458	0.1846	0.5773	0.3074	-1.4	-1.2	-1.3
tubulin gamma-2 chain / gamma-2 tubulin (TUBG2)	At5g05620	2685	1470	2333	1452	2301	1461	1956	1149	0.8283	0.8151	0.5464	-1.1	-1.1	-1.3

b

Name	Locus	DIS1_0d	DIS2_0d	DIS1_2d	DIS2_2d	DIS1_4d	DIS2_4d	DIS1_6d	DIS2_6d	p-value (T0-2d)	p-value (T0-4d)	p-value (T0-6d)	fold (T0-2d)	fold (T0-4d)	fold (T0-6d)
tubulin alpha-1 chain (TUA1)	At1g64740	4682	4171	10107	8249	11022	7719	8497	5821	0.0387	0.0978	0.1827	2.1	2.1	1.6
tubulin alpha-2/alpha-4 chain (TUA2)	At1g50010	15917	12461	9958	5374	5261	3188	8603	5112	0.1510	0.0385	0.0963	-1.9	-3.4	-2.1
tubulin alpha-3/alpha-5 chain (TUA3)	At5g19770	30458	23842	16869	8180	11619	5996	11299	6472	0.1157	0.0517	0.0468	-2.2	-3.1	-3.1
tubulin alpha-2/alpha-4 chain (TUA4)	At1g04820	20698	26107	10101	6182	4673	3424	9562	4608	0.0447	0.0200	0.0470	-2.9	-5.8	-3.3
tubulin alpha-3/alpha-5 chain (TUA5)	At5g19780	30084	25065	15598	8127	8507	5550	11350	6690	0.0731	0.0195	0.0324	-2.3	-3.9	-3.1
tubulin alpha-6 chain (TUA6)	At4g14960	45753	57751	25102	16331	13268	12050	25676	16548	0.0528	0.0230	0.0555	-2.5	-4.1	-2.5
tubulin beta-1 chain (TUB1)	At1g75780	204	252	253	206	183	140	166	183	0.9684	0.1751	0.1704	1.0	-1.4	-1.3
tubulin beta-2/beta-3 chain (TUB2)	At5g62690	17670	21520	19541	15221	12188	8276	14389	8255	0.5241	0.0762	0.1497	-1.1	-1.9	-1.7
tubulin beta-2/beta-3 chain (TUB3)	At5g62700	619	587	453	527	644	363	488	401	0.1072	0.5545	0.0759	-1.2	-1.2	-1.4
tubulin beta-4 chain (TUB4)	At5g44340	16693	23372	25952	15372	11389	6456	13627	3441	0.9290	0.1159	0.1996	1.0	-2.2	-2.3
tubulin beta-5 chain (TUB5)	At1g20010	6306	6006	2954	1710	1329	601	1353	753	0.0269	0.0057	0.0043	-2.6	-6.4	-5.8
tubulin beta-6 chain (TUB6)	At5g12250	6301	7241	9817	4570	4178	1710	2711	1084	0.8886	0.1013	0.0352	1.1	-2.3	-3.6
tubulin beta-7 chain (TUB7)	At2g29550	982	1482	697	626	551	611	670	538	0.1524	0.1227	0.1358	-1.9	-2.1	-2.0
tubulin beta-8 chain (TUB8) (TUBB8)	At5g23860	12561	18808	7395	10657	7243	8334	7409	8926	0.1994	0.1304	0.1443	-1.7	-2.0	-1.9
tubulin beta-9 chain (TUB9)	At4g20890	6573	10677	8173	6301	6058	4356	4234	4482	0.6010	0.2638	0.1736	-1.2	-1.7	-2.0
tubulin gamma-1 chain / gamma-1 tubulin (TUBG1)	At3g61650	667	507	362	665	408	626	334	520	0.7097	0.6562	0.3220	-1.1	-1.1	-1.4
tubulin gamma-2 chain / gamma-2 tubulin (TUBG2)	At5g05620	1938	1156	1388	1786	1076	1006	767	1066	0.9357	0.3264	0.2710	1.0	-1.5	-1.7

Supp Figure 1

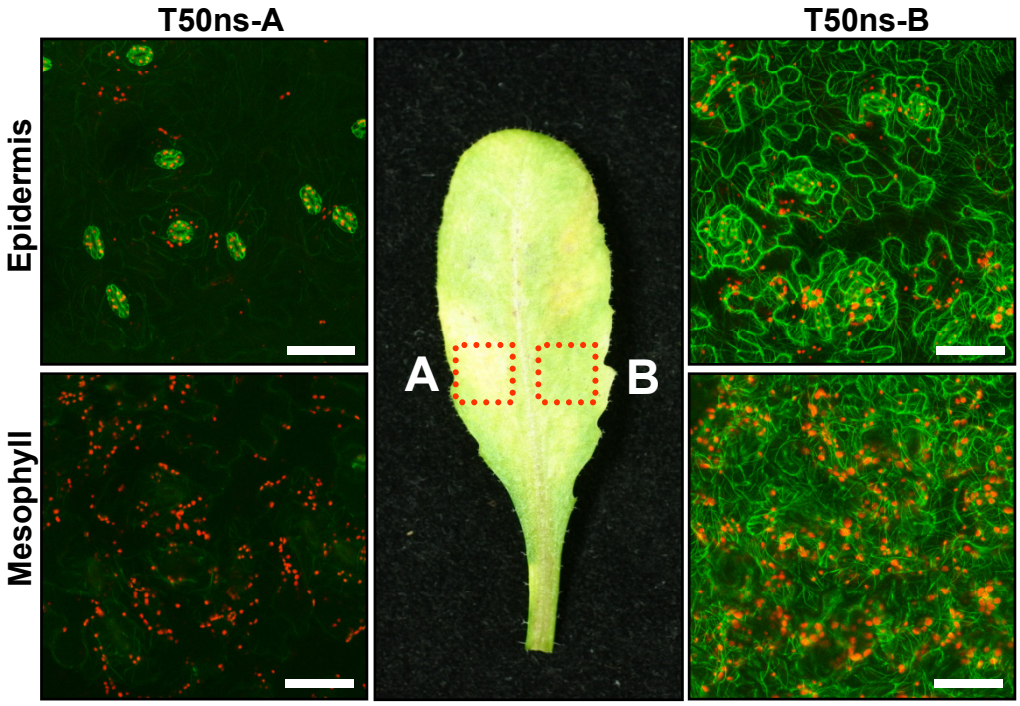

Supplemental figure 1. T50ns as an example of the heterogeneity in the degradation of the microtubule lattice during natural leaf senescence**.** Scale bars for panel B = 50µm

Supp Figure 2

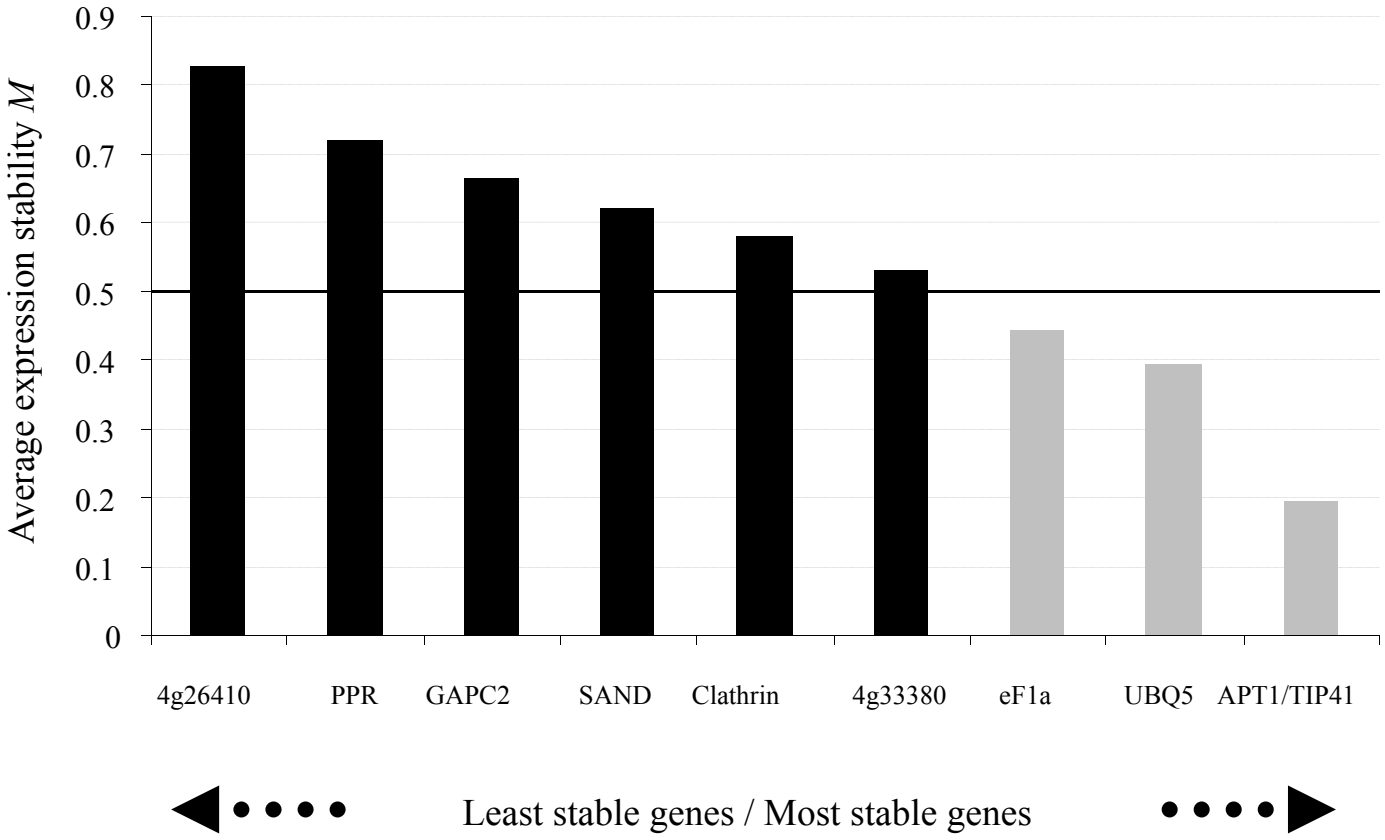

Supplemental figure 2. Validation of the reference genes (GeNorm) for the qRT-PCR analyses. Grey bars represent the average expression stability of the validated genes. All locus numbers are available in supp. table 2.